

LOW ENERGY QUARK-GLUON PROCESSES FROM EXPERIMENTAL DATA USING THE GLOBAL COLOUR MODEL^{*}

Reginald T. Cahill and Susan M. Gunner[†]

Department of Physics, Flinders University
GPO Box 2100, Adelaide 5001, Australia

Abstract

The Global Colour Model(GCM) of QCD is used to extract low energy quark-gluon processes from experimental data. The resultant effective quark-quark coupling correlator is compared with that of Jain and Munczek, and with the combined lattice results of Marenzoni *et al.* and Skullerud, and with the two-loop form. The results suggest that higher order gluon vertices are playing a role in coupling quark currents. The success of the GCM is explained by an infrared saturation effect.

Keywords: Quantum Chromodynamics, Global Colour Model, Quark-Gluon Coupling

PACS numbers: 12.38.Lg, 12.38.Aw, 12.38.Gc

1 Introduction

We report on the current status of the project extracting low energy quark-gluon processes from experimental data using the Global Colour Model[1] (GCM) of QCD. A new GCM fit (GCM98) to more extensive experimental data is reported here; this updates previous fits GCM95 and GCM97. The effective quark-quark coupling correlator is compared with that of Jain and Munczek[2], with the combined lattice results of Marenzoni *et al.*[3] and Skullerud[4], and with the two-loop form. The results show that this correlator agrees remarkably well with that of Jain and Munczek, and with one constructed from the Marenzoni *et al.* and Skullerud lattice

^{*}Contribution to the Workshop on Methods of Non-Perturbative Field Theory, Adelaide, Australia 2-13 Feb 1998.

[†]E-mail: Reg.Cahill@flinders.edu.au, Susan.Gunner@flinders.edu.au

results down to $s = 1.8\text{GeV}^2$. But, significantly, all three of these depart from the two-loop form below $s = 2.5\text{GeV}^2$. The difference between GCM98 - Jain-Munczek and the lattice construction below $s = 1.8\text{GeV}^2$ could be an indication of contributions to the quark-quark coupling at low energy from $n \geq 4$ gluon vertices.

2 Global Colour Model

The GCM modelling of QCD is based on the idea that as hadronic correlators are given by explicit functional integrals it should be possible, after an appropriate change of variables of integration, to identify a dominant configuration. It turns out that this dominant configuration is nothing more than the constituent quark(CQ) effect allowing QCD to be directly related to low energy hadronic physics. There are a number of reviews of the GCM[5, 6, 7, 8, 9]. In the functional integral approach correlators are defined by

$$\mathcal{G}(\dots, x, \dots) = \frac{\int D\bar{q}DqDAD\bar{C}DC\dots q(x)\dots\exp(-S_{QCD}[A, \bar{q}, q, \bar{C}, C])}{\int D\bar{q}DqDAD\bar{C}DC\exp(-S_{QCD}[A, \bar{q}, q, \bar{C}, C])}. \quad (1)$$

The various complete (denoted by scripted symbols) correlators \mathcal{G} lead to experimental observables. They are related by an infinite set of coupled Dyson-Schwinger Equations (DSE), and by the Slavnov-Taylor gauge-symmetry related identities and, in the chiral limit, to the axial Ward-Takahashi identity (AWTI). The usual truncation of these DSE causes the violation of all these identities, and in particular of the AWTI leading to spurious effects for the dynamical breaking of chiral symmetry which is critical to low energy hadronic physics. One remedy for the AWTI problem is to modify the quark DSE so that, in conjunction with the meson equations, the AWTI is satisfied. The GCM avoids this AWTI problem as it does not derive from these DSE; rather its nature follows from an analytical continuum estimation procedure for the functional integrations in which the AWTI is automatically satisfied. The correlators in Eq.(1) may be extracted from the generating functional of QCD,

$$Z_{QCD}[\bar{\eta}, \eta, J] = \int D\bar{q}DqDAD\bar{C}DC\exp(-S_{QCD}[A, \bar{q}, q, \bar{C}, C] + \bar{\eta}q + \bar{q}\eta + JA). \quad (2)$$

Functional transformations lead[5] to the GCM; briefly and not showing source terms for convenience, the gluon and ghost integrations are formally performed

$$\begin{aligned} \int D\bar{q}DqDAD\bar{C}DC\exp(-S_{QCD}) &= \int D\bar{q}Dq\exp(-\int \bar{q}(-\gamma.\partial + \mathcal{M})q + \\ &+ \frac{g_0^2}{2} \int j_\mu^a(x)j_\nu^a(y)\mathcal{G}_{\mu\nu}(x-y) + \frac{g_0^3}{3!} \int j_\mu^a j_\nu^b j_\rho^c \mathcal{G}_{\mu\nu\rho}^{abc} + \dots), \end{aligned} \quad (3)$$

where $j_\mu^a(x) = \bar{q}(x)\frac{\lambda^a}{2}\gamma_\mu q(x)$, g_0 is the bare coupling constant, and $\mathcal{G}_{\mu\nu}(x)$ is the gluon correlator with no quark loops but including ghosts (\bar{C}, C)

$$\mathcal{G}_{\mu\nu}(x-y) = \frac{\int DAD\bar{C}DCA_\mu^a(x)A_\nu^a(y)\exp(-S_{QCD}[A, \bar{C}, C])}{\int DAD\bar{C}DC\exp(-S_{QCD}[A, \bar{C}, C])}. \quad (4)$$

Fig.1 shows successive terms in Eq.(3). The terms of higher order than the term quartic in the quark fields are difficult to explicitly retain in any analysis. However the GCM models the effect of higher order terms by replacing the coupling constant g_0 by a momentum dependent quark-gluon coupling $g(s)$, and neglecting terms like $\mathcal{G}_{\mu\nu\rho}^{abc}$ and higher order in Eq.(3). This $g(s)$ is a

restricted form of vertex function. The modification $g_0^2 \mathcal{G}_{\mu\nu}(p) \rightarrow D_{\mu\nu}(p) = g(p^2) \mathcal{G}_{\mu\nu}(p) g(p^2)$ and the truncation then defines the GCM. We also call this effective quark-quark coupling correlator $D_{\mu\nu}(p)$ the effective gluon correlator.

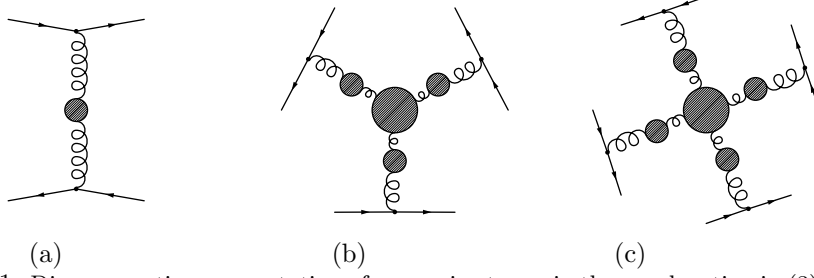


Figure 1: Diagrammatic representation of successive terms in the quark action in (3). The quark-gluon vertex strength is g_0 , while the gluon-gluon vertices (including gluon correlators) are fully dressed except for quark loops.

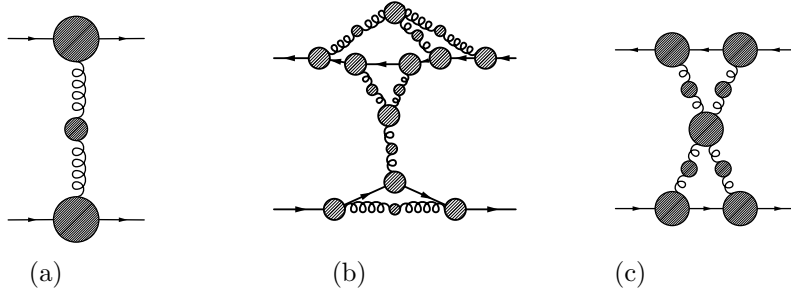


Figure 2: (a) The GCM effective $D_{\mu\nu}$ in (5), (b) example of correlations formally included in (a), and in (c) an $n = 4$ process not formally included in (a), but which is modelled in the GCM via the specific form of $D_{\mu\nu}$.

The GCM is equivalent to using a quark-gluon field theory with the action

$$S_{GCM}[A, \bar{q}, q] = \int \left(\bar{q}(-\gamma \cdot \partial + \mathcal{M} + i A_\mu^a \frac{\lambda^a}{2} \gamma_\mu) q + \frac{1}{2} A_\mu^a D_{\mu\nu}^{-1}(i\partial) A_\nu^a \right). \quad (5)$$

Here $D_{\mu\nu}^{-1}(p)$ is the matrix inverse of the Fourier transform of $D_{\mu\nu}(x)$ and Fig.2 shows processes formally included in $D_{\mu\nu}(p)$. This action is invariant under $q \rightarrow Uq, \bar{q} \rightarrow \bar{q}U^\dagger$, and $A_\mu^a \lambda^a \rightarrow UA_\mu^a \lambda^a U^\dagger$ (where U is a global 3×3 unitary colour matrix) - the global colour symmetry of the GCM. The gluon self-interactions that arise as a consequence of the local colour symmetry in Eq.(4) and the ghost and vertex effects lead to $D_{\mu\nu}^{-1}(p)$ being non-quadratic. Hence, in effect, the GCM models the QCD local gluonic action $\int F_{\mu\nu}^a[A] F_{\mu\nu}^a[A]$ in S_{QCD} of Eq.(1) which has local colour symmetry, by a highly nonlocal action in the last term of Eq.(5) which has global colour symmetry. It is important to appreciate that while the GCM has a formal global colour symmetry the detailed dynamical consequences of the local colour symmetry of QCD are modelled by the detailed form of $D(s)$. Approximations to the truncated DSE usually map QCD onto the GCM, as indicated in Fig.3. The success of this GCM modelling has been amply demonstrated [5, 6, 7, 8, 10].

Hadronisation[5] of the functional integrations in Eq.(1) involves a sequence of changes of variables involving, in part, the transformation to bilocal boson fields, and then to the usual local hadron fields (sources not shown):

$$Z \approx \int D\bar{q} Dq D A \exp(-S_{GCM}[A, \bar{q}, q] + \bar{\eta} q + \bar{q} \eta) \quad (\text{GCM})$$

$$= \int D\mathcal{B}D\overline{\mathcal{D}}D\exp(-S[\mathcal{B},\overline{\mathcal{D}},\mathcal{D}]) \quad (\text{bilocal fields}) \quad (6)$$

$$= \int D\overline{N}DN..D\pi D\rho D\omega...\exp(-S_{had}[\overline{N}, N, ..\pi, \rho, \omega....]) \quad (\text{local fields}) . \quad (7)$$

The bilocal fields in Eq.(6) arise naturally and correspond to the fact that, for instance, mesons are extended states. This hadronisation derives from functional integral calculus changes of variables which are induced by generalised Fierz transformations that emerge from the colour, spin and flavour structure of QCD. The final functional integrations in Eq.(7) over the hadrons give the hadronic observables, and are equivalent to dressing each constituent hadron by, mainly, lighter constituent mesons. The basic insight is that the quark-gluon dynamics, in Eq.(1), is fluctuation dominated, whereas the hadronic functional integrations in Eq.(7) are not. The induced hadronic effective action in Eq.(7) is nonlocal. The GCM automatically preserves the consequences of the dynamically broken chiral symmetry in the action in Eq.(7).

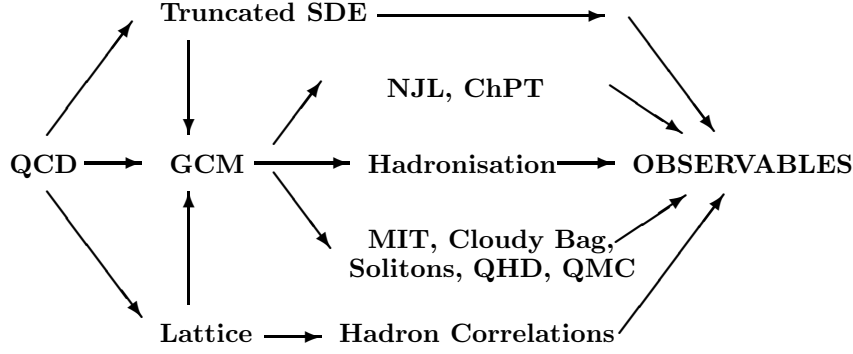


Figure 3: Relational map of the GCM to QCD and various other modellings including the Nambu - Jona-Lasinio (NJL), Quantum Hadrodynamics (QHD), Quark Meson Coupling (QMC) and Chiral Perturbation Theory (ChPT).

A key idea in the GCM is that in proceeding from Eq.(6) to Eq.(7) one expands $S[\mathcal{B},..]$ about the configuration \mathcal{B}_{CQ} that minimises it, giving in Eq.(9) the GCM Constituent Quark (CQ) equations,

$$\frac{\delta S}{\delta \mathcal{B}(x, y)} \big|_{\mathcal{B}_{CQ}} = 0 . \quad (8)$$

Thus for *all* hadrons one assumes a universal dominant configuration. This amounts to assuming that all hadrons share a common dynamical feature. Of the set $\mathcal{B}(x, y)_{CQ}$ only $A(x - y)$ and $B(x - y)$ (their Fourier transforms appear in Eq.(10)) are non-zero translation-invariant bilocal fields characterising the dominant configuration. This is the dynamical breaking of chiral symmetry. The dominant configuration is analogous to the condensate of Cooper pairs in the BCS theory of superconductivity. However unlike solid state superconductivity here there is no normal component. Writing out the translation invariant CQ equations we find that the dominant configuration is indeed simply the constituent quark effect as they may be written in the form,

$$G^{-1}(p) = i\not{p} + m + \frac{4}{3} \int \frac{d^4 q}{(2\pi)^4} D_{\mu\nu}(p - q) \gamma_\mu G(q) \gamma_\nu, \quad (9)$$

and we see that this is the gluon dressing of a constituent quark. This equation is *exact* in the GCM and its solution has the structure

$$G(q) = (iA(q)q \cdot \gamma + B(q) + m)^{-1} = -iq \cdot \gamma \sigma_v(q) + \sigma_s(q). \quad (10)$$

In the chiral limit there are more \mathcal{B}_{CQ} fields that are non-zero, and the resultant degeneracy of the dominant configuration is responsible for the masslessness of the pion. The constituent quark correlator G should not be confused with the complete quark correlator \mathcal{G} from Eq.(1). This \mathcal{G} would be needed to analyse the existence or otherwise of free quarks. The G on the other hand relates exclusively to the internal structure of hadrons, and to the fact that this appears to be dominated by the constituent quark effect. The evaluation of \mathcal{G} is a very difficult task, even within the GCM while G is reasonably easy to study using Eq.(9). The truncation of the DSE in which the full quark \mathcal{G} is approximated by the CQ G amounts to using a mean field approximation; however the truncated DSE then has no systematic formalism for going beyond the mean field as in the GCM. The hadronic effective action in Eq.(7) arises when $S[\mathcal{B}, ..]$ is expanded about the dominant CQ configuration; the first derivative is zero by Eq.(8), and the second derivatives, or curvatures, give the constituent or core meson correlators $G_m(q, p; P)$

$$G_m^{-1}(q, p; P) = F.T. \left(\frac{\delta^2 S}{\delta \mathcal{B}(x, y) \delta \mathcal{B}(u, v)} \Big|_{\mathcal{B}_{CQ}} \right), \quad (11)$$

after exploiting translation invariance and Fourier transforming. Higher order derivatives lead to couplings between the meson cores. The $G_m(q, p; P)$ are given by ladder-type correlator equations. The non-ladder effects are inserted by the final functional integrals in Eq.(7), giving the complete GCM meson correlators $\mathcal{G}_m(q, p; P)$. It is interesting to note that the truncated and modified DSE in Maris and Roberts[13] are identical to Eq.(9) and Eq.(11) (in the form of Eq.(12)). However Maris and Roberts[13] assume that $D(s)$ has the two loop form down to $s \approx 1\text{GeV}^2$, and this assumption is not supported by the detailed analyses reported herein. An important advantage of the GCM modelling of QCD is that the hadronic sector effective action is manifestly derivable. One key feature is that the meson exchange within the diquark subcorrelations of the baryon correlators is seen to insert crossed gluonic exchanges, and these appear to stop the diquark correlations from developing a mass-shell, i.e. the diquark correlations are confined[14].

In the present analysis the ω and a_1 mesons are described by these constituent meson correlators; that is, we ignore meson dressings of these mesons. The mass M of these states is determined by finding the pole position of $G_m(q, p; P)$ in the meson momentum $P^2 = -M^2$ and this leads to the homogeneous vertex equation

$$\Gamma(p; P) = -\frac{4}{3} \int \frac{d^4 q}{(2\pi)^4} D_{\mu\nu}(q - p) \gamma_\mu G(q + \frac{P}{2}) \Gamma(q; P) G(q - \frac{P}{2}) \gamma_\nu. \quad (12)$$

The success of the GCM appears to be based on the phenomenon of an IR saturation mechanism in which the extreme IR strength of the many contributing quark-quark couplings is easily modelled by this one effective gluon correlator $D_{\mu\nu}(p)$. Of particular dynamical interest is the comparison of the GCM $D_{\mu\nu}(p)$ with one constructed theoretically from only a gluon correlator and vertex functions, say from continuum or lattice modellings, for this gives some insight into the IR strength of the higher order gluonic couplings.

3 Procedures

To solve Eq.(9) for various $D_{\mu\nu}(p)$ and then to proceed to use $A(s)$ and $B(s)$ in meson correlator equations for fitting observables to meson data is particularly difficult. A robust numerical

technique is to use a separable expansion[10].

$$D_{\mu\nu}(p) = (\delta_{\mu\nu} - \frac{p_\mu p_\nu}{p^2})D(p^2), \quad \text{and} \quad \mathcal{G}_{\mu\nu}(p) = (\delta_{\mu\nu} - \frac{p_\mu p_\nu}{p^2})\mathcal{G}(p^2). \quad (13)$$

We expand $D(p - q)$ in Eq.(9) into $O(4)$ hyperspherical harmonics

$$D(p - q) = D_0(p^2, q^2) + q \cdot p D_1(p^2, q^2) + \dots, \quad (14)$$

$$D_0(p^2, q^2) = \frac{2}{\pi} \int_0^\pi d\beta \sin^2 \beta D(p^2 + q^2 - 2pq \cos \beta), \dots \quad (15)$$

We then introduce multi-rank separable D_0 expansion (here $n = 3$):

$$D_0(p^2, q^2) = \sum_{i=1, n} \Gamma_i(p^2) \Gamma_i(q^2). \quad (16)$$

The constituent quark equations then have solutions of the form

$$B(s) = \sum B_i(s), \quad B_i(s) = b_i \Gamma_i(s), \quad \sigma_s(s) = \sum_{i=1, n} \sigma_s(s)_i, \quad (17)$$

$$b_i^2 = 4\pi^2 \int_0^\infty s ds B_i(s) \sigma_s(s), \quad \text{and} \quad B_i(s) = \frac{\sigma_s(s)_i}{s \sigma_v(s)^2 + \sigma_s(s)^2}, \quad (18)$$

However rather than specifying Γ_i in (16) we proceed by parametrising forms for the σ_{si} and σ_v ; the Γ_i then follow from (17) and (18):

$$\begin{aligned} \sigma_s(s)_1 &= c_1 \exp(-d_1 s), \quad \sigma_s(s)_2 = c_2 \cdot \left(\frac{2s^2 - d_2(1 - \exp(-2s^2/d_2))}{2s^4} \right)^2, \\ \sigma_s(s)_3 &= c_3 \left(\frac{2f(s) - d_3(1 - \exp(-2f(s)/d_3))}{2f(s)^2} \right)^2, \quad f(s) = s(\ln(\tau + s/\Lambda^2))^{1/2}, \\ \sigma_v(s) &= \frac{2s - \beta^2(1 - \exp(-2s/\beta^2))}{2s^2}. \end{aligned} \quad (19)$$

The three σ_{si} terms mainly determine the IR, midrange and UV regions; the $\sigma_s(s)_3$ term describes the asymptotic form of $\sigma_s(s) \sim 1/s^2 \ln(s/\Lambda^2)$ for $s \rightarrow \infty$ and ensures the form for $D(s) \sim 1/s \ln(s/\Lambda^2)$. With these parametrised forms we can numerically relate the mass of the $a_1(1230\text{MeV})$ and $\omega(783\text{MeV})$ mesons from Eq.(12), $f_\pi(93.3\text{MeV})$ and experimental points for $\alpha(s)$ (see Fig.4a insert) from the Particle Data Book for $s > 3\text{GeV}^2$ to the parameter set in Table 1 in a robust and stable manner.

Table 1: $\sigma_s(s)$ and $\sigma_v(s)$ Parameters.

c_1	1.839GeV^{-1}	d_1	3.620GeV^{-2}	β	0.4956GeV
c_2	0.0281GeV^7	d_2	1.516GeV^4	Λ	0.234GeV
c_3	0.0565GeV^3	d_3	0.7911GeV^2		

The translation invariant form for the effective gluon correlator is easily reconstructed by using $D(p^2) = D_0(p^2, 0)$ from Eq.(15)

$$D(p^2) = \sum_i \frac{1}{b_i^2} \frac{\sigma_s(0)_i}{\sigma_s(0)^2} \frac{\sigma_s(p^2)_i}{p^2 \sigma_v(p^2)^2 + \sigma_s(p^2)^2}. \quad (20)$$

With the parameter set in Table 1 the resulting $D(p^2)$ is shown in Fig.4. Shown in Fig.4a is the pure gluon correlator $\mathcal{G}(p^2)$ from the lattice calculations of Marenzoni *et al* [3], corresponding

to the value $\beta = 6.0$, where the errors arise mainly from a 5% uncertainty in the lattice spacing; $a = 0.50 \pm 0.025 \text{ GeV}^{-1}$. A significant feature of QCD is that the infrared dominance, as revealed by the large value of $D(s)$ at small s , causes the CQ equations to saturate, i.e. the form of the solutions $A(s)$ and $B(s)$ is independent of the detailed IR form of $D(s)$. This saturation effect means that low energy QCD is surprisingly easy to model.

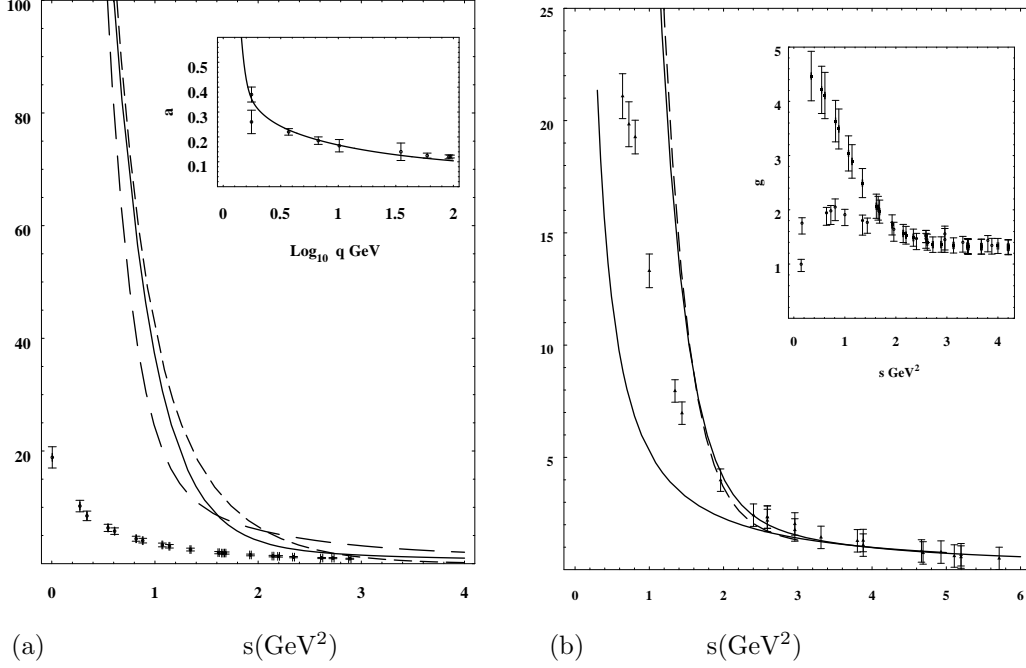


Figure 4: Plots of $D(s)$ (GeV^{-2}). In (a) solid line is GCM98; shortdash line is GCM95; longdash line is GCM97. Data plot is lattice pure-gluon $\mathcal{G}(s)$ from Marenzoni *et al.*, and so has no quark-gluon vertex. Insert is fit of GCM98 to $\alpha(s)$ of Particle Data Book. In (b) GCM98 is the solid line; dashed line is Jain and Munczek; lower solid line is two-loop form with $\Lambda = 0.234 \text{ GeV}$ and $N_f = 3$; data plot is combined lattice data for $g(s)\mathcal{G}(s)g(s)$ with $\mathcal{G}(s)$ from Marenzoni *et al.* (as in (a)) and $g(s)$ from Skullerud. Insert shows $g(s)$ from Skullerud (lower data plot), and from GCM98/ $\mathcal{G}(s)$ (upper data plot).

Also shown in Fig.4(a) are the earlier GCM fits: GCM95[10] and GCM97[11]. The insert in Fig.4(a) shows the GCM98 in the form of $\alpha(q)$ ($D(s) = \frac{4\pi\alpha(s)}{s}$) compared with experimental data from the Particle Data Book. In Fig.4(b) we show the new GCM98 quark-quark correlator $D(s)$ showing excellent agreement with the Jain-Munczek[2] $D(s)$, and with one constructed from the Marenzoni *et al.* and Skullerud lattice results down to $s = 1.8 \text{ GeV}^2$; $D(s) = g(s)\mathcal{G}(s)g(s)$. The normalisation and shape of the Marenzoni *et al.* $\mathcal{G}(s)$ agrees with that of Leinweber *et al.*[15]. However the normalisation of the much more difficult lattice computation of $g(s)$ is uncertain and we have chosen it so that the combined lattice $D(s)$ agrees with the experimental Particle Data Book for $s > 3 \text{ GeV}^2$. As shown in Fig.4(b) all three of these depart from the two-loop form below $s = 2.5 \text{ GeV}^2$. The difference between GCM98 - Jain-Munczek and the lattice construction could be an indication of contributions to the quark-quark coupling from $n \geq 4$ gluon self-couplings at low energy, since processes like Fig.2(c) would be included in the GCM fit, but are not in the lattice construction.

The insert in Fig.4(b) shows the $g(s)$ from $g^2(s) = D(s)/\mathcal{G}(s)$ that then follows from our analysis. This is the effective quark-gluon coupling vertex if the gluon correlator is taken to be that of Marenzoni *et al.* or Leinweber *et al.*. Here the error bars now indicate combined errors and uncertainties from the lattice spacing. Also shown is $g(s)$ from Skullerud[4] with the normalisation as discussed above.

The GCM95-GCM98 parametrisations differed mainly in their asymptotic forms, and when fitting to meson data these differences only resulted in slight variations of $D(s)$ for intermediate s values, as shown in Fig.4(a). The consequent small variations in the predicted values of various hadronic properties are shown in Table 2. However forcing the asymptotic form to fit experimental data for $D(s)$ even for $s > 3\text{GeV}^2$ results in a stabilisation of the GCM $D(s)$.

Table 2: Hadronic Observables.

Observable	GCM1995	GCM1997	GCM1998	Expt./Theory
f_π	93.0MeV*	93.2MeV*	92.40MeV*	93.3MeV
a_1 meson mass	1230MeV*	1231MeV*	1239MeV*	1230MeV
π meson mass(for $m_{u,d}$)	138.5MeV*	138.5MeV*	138.5MeV*	138.5MeV
$\alpha(q)$	-	-	see fig.4a	†
K meson mass (for m_s only)	496MeV*	-	-	496MeV
$(m_u + m_d)/2 _R(\mu = 1\text{GeV})$	6.5MeV	4.8MeV	7.7MeV	$\approx 8.0\text{MeV}$
$m_s _R(\mu = 1\text{GeV})$	135MeV	-	-	130MeV
ω meson mass	804MeV	783MeV*	783MeV*	782MeV
$a_0^0 \pi - \pi$ scatt. length	0.1634	0.1622	0.1657	0.26 ± 0.05
$a_0^2 \pi - \pi$ scatt. length	-0.0466	-0.0463	-0.0465	-0.028 ± 0.012
$a_1^1 \pi - \pi$ scatt. length	0.0358	0.0355	0.0357	0.038 ± 0.002
$a_2^0 \pi - \pi$ scatt.length	0.0017	0.0016	0.0018	0.0017 ± 0.003
$a_2^2 \pi - \pi$ scatt.length	-0.0005	-0.0005	-0.0003	0.00013 ± 0.0003
r_π pion charge radius	0.55fm	0.53fm	0.53fm	0.66fm
$\frac{1}{2}^+(0^+)$ nucleon-core mass**	1390MeV	1435MeV	1450MeV	$>1300\text{MeV} \dagger\dagger$
constituent quark rms size	0.51fm	0.39fm	0.58fm	-
chiral quark constituent mass	270MeV	267MeV	325MeV	-
0^+ diquark rms size	0.55fm	0.55fm	0.59fm	-
0^+ diquark const. mass	692MeV	698MeV	673MeV	$>400\text{MeV}$
1^+ diquark const. mass	1022MeV	903MeV	933MeV	-
0^- diquark const. mass	1079MeV	1049MeV	1072MeV	-
1^- diquark const. mass	1369MeV	1340MeV	1373MeV	-
MIT bag constant	$(154\text{MeV})^4$	$(145\text{MeV})^4$	$(166\text{MeV})^4$	$(146\text{MeV})^4$
MIT N-core (no cms corr.)	1500MeV	1420MeV	1625MeV	$>1300\text{MeV} \dagger\dagger$
* fitted observable; - not computed or not known; † $\alpha(s)$ from Particle Data Book; GCM1995: Cahill and Gunner[10]; GCM1997: Cahill and Gunner[11]; GCM1998: this report. ** only 0^+ diquark correlation; 1^+ diquark correlation lowers nucleon core mass. †† nucleon core mass (i.e. no meson dressing).				

4 Conclusion

Figs.4(a) and 4(b) reveal that the GCM95-98 project of extracting low energy quark-gluon processes has reached a stage where some detailed insights are emerging. It is clear that the continuum modelling, when fitted to experimental data, leads to a unique quark-quark coupling correlator. This is shown by the excellent agreement between the GCM multi-rank technique

and the Jain-Munczek result[2, 12]. This continuum result is also in excellent agreement with the combined lattice prediction down to $s \approx 1.8\text{GeV}^2$. All three results show a clear departure from the two-loop form below $s = 2.5\text{GeV}^2$. The difference between the GCM modelling and the combined lattice $D(s)$ at lower s values raises an interesting interpretation. Assuming that the lattice calculation of $g(s)$ is confirmed by future studies, particularly at low s , we must conclude that the GCM analysis of the experimental data is revealing the influence of processes that are not in the lattice construct. The most obvious possibility is that the high order gluon vertices, as in Fig.2(c), are contributing at low energies, and providing additional attractive interaction between quark currents. Provided these contribute only in the region where $D(s)$ is large the detailed form of these contributions is not needed since the saturation effect means that hadronic observables are independent of these details, including their gauge dependence. Thus the saturation of the constituent quark processes and the related dynamical breaking of chiral symmetry explains why the GCM works so well as a low-energy *equivalent* field theory for QCD.

References

- [1] R.T. Cahill and C.D. Roberts, *Phys. Rev. D* **32**, 2419(1985).
- [2] P. Jain and H.J. Munczek, *Phys. Rev. D* **48**, 5403(1993).
- [3] P. Marenzoni, G. Martinelli, and N. Stella, *Nucl.Phys. B* **455**, 339(1995).
- [4] J.I. Skullerud, *Nucl. Phys. Proc. Suppl.* **63**, 242(1998).
- [5] R.T. Cahill, *Nucl. Phys. A* **543**, 63c(1992).
- [6] C.D. Roberts and A.G. Williams, *Prog.Part.Nucl.Phys.* **33**, 477(1994).
- [7] R.T. Cahill and S.M. Gunner, *Aust. J. Phys.* **50**, 103(1997).
- [8] P.C. Tandy, *Prog. Part. Nucl. Phys.* **39**, 117(1997).
- [9] R.T. Cahill and S.M. Gunner, *Fizika B* **7**, 171(1998), hep-ph/9812491.
- [10] R.T. Cahill and S.M. Gunner, *Phys. Lett. B* **359**, 281(1995).
- [11] R.T. Cahill and S.M. Gunner, hep-ph/9711359.
- [12] D. Kekez and D. Klabučar, *Phys. Lett., B* **387**, 14(1996).
- [13] P. Maris and C.D. Roberts, *Phys. Rev. D* **56**, 3369(1997).
- [14] A. Bender, C.D. Roberts and L. Von-Smekal, *Phys.Lett. B* **380**, 7(1996).
- [15] D.B. Leinweber, J.I. Skullerud, A.G. Williams and C. Parrinello, *Phys. Rev. D* **58**, 031501(1998).